REPUBLIC OF TÜRKİYE
YILDIZ TECHNICAL UNIVERSITY
GRADUATE SCHOOL OF SCIENCE AND ENGINEERING

COMPARATIVE ANALYSIS OF CONTROLLER DESIGNS FOR PAN-TILT SYSTEM WITH RESPECT TO PERFORMANCE AND CONTROL EFFORT

Efe Yazıcı

MASTER OF SCIENCE THESIS

Department of Control and Automation Engineering
Program of Control and Automation Engineering

Supervisor
Assoc. Prof. Dr. Yavuz EREN

Aralık, 2025

REPUBLIC OF TÜRKİYE
YILDIZ TECHNICAL UNIVERSITY
GRADUATE SCHOOL OF SCIENCE AND ENGINEERING

COMPARATIVE ANALYSIS OF CONTROLLER DESIGNS FOR PAN-TILT SYSTEM WITH RESPECT TO PERFORMANCE AND CONTROL EFFORT

A thesis submitted by Efe Yazıcı in partial fulfillment of the requirements for the degree of **MASTER OF SCIENCE** is approved by the committee on 26.12.2025 in Department of Control and Automation Engineering, Program of Control and Automation Engineering.

Assoc. Prof. Dr. Yavuz EREN
Yildiz Technical University
Supervisor

Approved By the Examining Committee

Assoc. Prof. Dr. Yavuz EREN, Supervisor
Yildiz Technical University _____

Asst. Prof. Fatih ADIGÜZEL, Member
Yildiz Technical University _____

Asst. Prof. Onur AKBATI, Member
Istanbul Technical University _____

I hereby declare that I have obtained the required legal permissions during data collection and exploitation procedures, that I have made the in-text citations and cited the references properly, that I haven't falsified and/or fabricated research data and results of the study and that I have abided by the principles of the scientific research and ethics during my Thesis Study under the title of "Comparative Analysis of Controller Designs for Pan-Tilt System with Respect to Performance and Control Effort" supervised by my supervisor, Assoc. Prof. Dr. Yavuz EREN. In the case of a discovery of false statement, I am to acknowledge any legal consequence.

Efe Yazıcı

Signature

Dedicated to my family
and my best friend

Acknowledgements

I would like to express my sincere gratitude to my thesis advisor, Assoc. Prof. Yavuz EREN, for his invaluable guidance, patience, and continuous support throughout the course of this study. His expertise, encouragement, and insightful feedback have been fundamental to the successful completion of this thesis.

I am also thankful to the members of my thesis examining committee, Asst. Prof. Fatih ADIGÜZEL and Asst. Prof. Onur AKBATI, for their constructive criticism and valuable suggestions, which have contributed significantly to improving the quality of this work.

My heartfelt appreciation goes to Assoc. Prof. Claudia Fernanda YAŞAR, Asst. Prof. Buse TACAL UCUN, Res. Asst. Ammar URGAN, and Res. Asst. Kadircan KURTULUŞ for their guidance, support, and motivation during both my undergraduate and graduate studies. Their encouragement and academic mentorship have played an important role in shaping my academic development.

I am deeply indebted to my family for their unwavering love, patience, and understanding throughout this challenging journey. Finally, I would like to express my special thanks to Gülbin KIRIKOĞLU for her constant support, encouragement, and presence by my side during every stage of this process.

Efe Yazıcı

TABLE OF CONTENTS

LIST OF SYMBOLS vii

LIST OF ABBREVIATIONS ix

LIST OF FIGURES x

LIST OF TABLES xi

ABSTRACT xii

ÖZET xiii

1 INTRODUCTION 1

1.1 System Overview 1

1.2 Literature Review 3

1.3 Objective of the Thesis 5

1.4 Hypothesis 6

2 METHODOLOGY 7

2.1 Simulation Environment 8

2.2 Overall Workflow 8

3 PAN - TILT SYSTEM 10

3.1 System Description 10

3.1.1 Dynamic Model Of The Pan - Tilt Mechanism 11

3.1.2 Linearization of the Nonlinear Model 15

3.1.3 Linearized State–Space Representation 17

4 CONTROLLER DESIGN 19

4.1 Traditional Control Techniques 19

4.1.1 PD Controller 19

4.1.2 LQR Controller 20

4.2 Feedforward Gravity Compensation 21

4.3 Advanced Control Techniques 22

4.3.1 Lyapunov-Based Control Design 23

4.3.2 High-Gain Observer (HGO) Design 24

5 SIMULATION RESULTS 26

5.1 Linear Control Simulations 26

5.1.1 PD Controller 26

5.1.2 LQR Controller 27

5.2 Nonlinear Control Simulations 28

5.2.1 Gravity Compensation in Nonlinear Dynamics 28

5.2.2 PD Controller Performance 29

5.2.3 LQR Controller Performance 31

5.3 Lyapunov-Based Nonlinear Control Results 32

5.4 High Gain Observer (HGO) based CTC Implementation 35

5.5 Qualitative Analysis of Control Strategies 38

6 RESULTS AND COMPARATIVE DISCUSSION 39

6.1 Quantitative Comparison 39

6.2 Comparative Discussion 39

7 CONCLUSION 42

REFERENCES 44

PUBLICATIONS FROM THE THESIS 47

LIST OF SYMBOLS

$\dot{\theta}_1$, $\dot{\theta}_2$	Angular velocities of pan and tilt joints
u	Control input vector
R	Control weighting matrix (LQR)
C	Coriolis and centrifugal matrix
K_d	Derivative gain
d_2	Distance from tilt joint to center of mass
$\hat{y}$	Estimated output
$\hat{x}$	Estimated state vector
u_g	Gravity compensation torque
g	Gravitational acceleration (9.81 m/s^2)
L	High–Gain Observer (HGO) gain matrix
M	Inertia matrix
B	Input Jacobian matrix (linearized dynamics)
$\ddot{q}$	Joint acceleration vector
q	Joint position vector
$\dot{q}$	Joint velocity vector
l	Length of the connecting link (center of mass distance)
K	LQR feedback gain matrix
J	LQR performance index
V	Lyapunov candidate function
m_1, m_2	Masses of the pan and tilt links
y	Measured system output
τ_1, τ_2	Motor torques for pan and tilt

$f(x, u)$	Nonlinear state-space function
θ_1, θ_2	Pan and tilt joint angles
K_p	Proportional gain
A	State Jacobian matrix (linearized dynamics)
Q	State weighting matrix (LQR)
x	State vector
τ	General control torque input
e	Tracking error
K_v	Velocity feedback gain

LIST OF ABBREVIATIONS

CTC	Computed Torque Control
DoF	Degrees of Freedom
HGO	High–Gain Observer
LQR	Linear Quadratic Regulator
LTI	Linear Time–Invariant
MATLAB	Matrix Laboratory
MPC	Model Predictive Control
NN	Neural Network
PD	Proportional–Derivative Controller
PID	Proportional–Integral–Derivative Controller
PTZ	Pan–Tilt–Zoom
SMC	Sliding Mode Control
UAV	Unmanned Aerial Vehicle

LIST OF FIGURES

Figure 1.1 Example of a PTZ camera used in surveillance systems. **2**
Figure 1.2 Example of a UAV-mounted gimbal camera. **2**
Figure 1.3 Pan–tilt camera module used in robotic applications. **3**
Figure 2.1 Overall workflow of the methodology followed in this thesis. . . **9**
Figure 3.1 Coordinate frames of the two-axis Pan–Tilt mechanism (taken from [6]). **10**
Figure 3.2 Illustration of the equilibrium configuration. **15**
Figure 4.1 Feedforward scheme **22**
Figure 5.1 PD Controller — Linear Model **26**
Figure 5.2 LQR Controller — Linear Model **27**
Figure 5.3 PD Controller – Nonlinear Model (Without Compensation) . . . **29**
Figure 5.4 PD Controller – Nonlinear Model (With Gravity Compensation) **30**
Figure 5.5 LQR Controller – Nonlinear Model (Without Compensation) . . **31**
Figure 5.6 LQR Controller – Nonlinear Model (With Gravity Compensation) **32**
Figure 5.7 Response of $\phi(t)$. **33**
Figure 5.8 Response of $\theta(t)$. **33**
Figure 5.9 Control input $u_2(t)$. **34**
Figure 5.10 Lyapunov function $V(t)$. **34**
Figure 5.11 $\phi(t)$ response with HGO-CTC. **35**
Figure 5.12 $\theta(t)$ response with HGO-CTC. **36**
Figure 5.13 True and estimated $\dot{\phi}$ comparison. **36**
Figure 5.14 True and estimated $\dot{\theta}$ comparison. **37**
Figure 5.15 Torque $u_2(t)$ with HGO-CTC. **37**

LIST OF TABLES

Table 3.1 Physical parameters of the Pan–Tilt system[4] **14**
Table 6.1 Comparison of Controller Performance Metrics **39**

ABSTRACT

Comparative Analysis of Controller Designs for Pan-Tilt System with Respect to Performance and Control Effort

Efe Yazıcı

Department of Control and Automation Engineering
Master of Science Thesis

Supervisor: Assoc. Prof. Dr. Yavuz EREN

The pan–tilt system exhibits nonlinear dynamics, making precise control challenging. In this study, both nonlinear and linearized mathematical models of the system were derived. Based on the linear model, Proportional–Derivative (PD) and Linear Quadratic Regulator (LQR) controllers were designed and tested on both linearized and nonlinear models. Controller performance was evaluated in terms of system response, control effort, and practical applicability. To improve accuracy, gravity effects were modeled and compensated within the control structure. Simulations were carried out in MATLAB^{TM} using optimized gains for PD, LQR, and feedforward-compensated configurations. In the extended part of the study, a Lyapunov-based nonlinear controller and a High-Gain Observer (HGO) were developed to enhance stability and enable state estimation. Both linear and nonlinear control schemes were analyzed comparatively to assess their effectiveness and robustness.

Keywords: Pan–Tilt, Modeling, Linear Control, Nonlinear Control, Lyapunov, Observer, Simulation.

YILDIZ TECHNICAL UNIVERSITY
GRADUATE SCHOOL OF SCIENCE AND ENGINEERING

ÖZET

Pan ve Tilt Sistemi İçin Farklı Kontrolcü Tiplerinin Performans ve Kontrol Eforu Açısından Karşılaştırılması

Efe Yazıcı

Kontrol ve Otomasyon Mühendisliği Anabilim Dalı
Yüksek Lisans Tezi

Danışman: Doç. Dr. Yavuz EREN

Pan–tilt sistemi doğrusal olmayan bir dinamiğe sahiptir ve bu durum sistemin hassas bir şekilde kontrol edilmesini zorlaştırmaktadır. Bu çalışmada, sistemin hem doğrusal olmayan hem de doğrusal hale getirilmiş matematiksel modelleri elde edilmiştir. Doğrusal model temel alınarak Oransal–Türev (PD) ve Lineer Kare Regülatör (LQR) denetleyiciler tasarlanmış ve her iki model üzerinde test edilmiştir. Denetleyicilerin performansı, sistem cevabı, kontrol eforu ve uygulanabilirlik açısından değerlendirilmiştir. Doğruluk artırmak amacıyla, yerçekimi etkisi modele dahil edilerek kontrol yapısında telafi edilmiştir. MATLAB^{TM} ortamında PD, LQR ve ileri beslemeli (feedforward) denetleyici yapılarına ait kazançlar optimize edilerek benzetimler gerçekleştirilmiştir. Çalışmanın genişletilmiş kısmında, sistem kararlılığını artırmak ve durum kestirimi sağlamak amacıyla Lyapunov tabanlı doğrusal olmayan bir denetleyici ve Yüksek Kazançlı Gözleyici (High-Gain Observer, HGO) tasarlanmıştır. Elde edilen doğrusal ve doğrusal olmayan denetim yapılarının etkinlik ve dayanıklılık açısından karşılaştırmalı analizi yapılmıştır.

Anahtar Kelimeler: Pan–Tilt, Modelleme, Doğrusal Kontrol, Doğrusal Olmayan Kontrol, Lyapunov, Gözleyici, Benzetim.

YILDIZ TEKNİK ÜNİVERSİTESİ
FEN BİLİMLERİ ENSTİTÜSÜ

1
INTRODUCTION

1.1 System Overview

The pan–tilt system is a mechanical platform consisting of two orthogonal rotational axes: the horizontal (pan) axis and the vertical (tilt) axis. Each axis is typically actuated by servo or DC motors equipped with gear reduction mechanisms to provide sufficient torque and positioning accuracy. The mechanical structure is composed of lightweight yet rigid components such as aluminum brackets, precision bearings, and shaft couplers, which ensure smooth rotation and high structural stability. Although the axes are arranged to allow largely independent motion, inertia coupling and gravitational effects introduce nonlinear dynamic behavior, particularly in the tilt axis. The incorporation of angular encoders or position sensors enables accurate feedback control, forming the foundation for high-performance motion regulation.

The mechanical characteristics of the system significantly influence its overall dynamic response and controller performance. Parameters such as mass distribution, link lengths, joint friction, and motor properties must be accurately identified to establish a reliable mathematical model. In particular, gravitational torque on the tilt axis introduces strong nonlinearities that require compensation either through feedforward methods or advanced nonlinear controllers. Additionally, mechanical imperfections such as backlash in the gear train or joint tolerances may lead to oscillations or steady-state errors, making robust and adaptive control strategies essential for real-world implementations.

Pan–tilt mechanisms are widely used in security and surveillance applications, where dynamic camera positioning is required to monitor large areas (see Fig. 1.1). PTZ (pan–tilt–zoom) cameras enable remote orientation control, allowing operators to scan environments, track moving targets, and maintain continuous situational awareness.



Figure 1.1 Example of a PTZ camera used in surveillance systems.

A PTZ surveillance camera capable of remote pan and tilt motion, providing wide-area coverage in monitoring applications [1].

Similarly, pan–tilt mechanisms are also widely employed in defense and aerospace systems, particularly in gimbal units mounted on unmanned aerial vehicles (UAVs) (see Fig. 1.2). These platforms enable stabilized and precise directional control of onboard cameras and sensors, providing reliable imaging and target tracking even under dynamic flight conditions.



Figure 1.2 Example of a UAV-mounted gimbal camera.

A stabilized gimbal camera designed for UAV applications, providing precise pan and tilt motion for electro-optical and infrared imaging [2].

In addition, pan–tilt systems are frequently utilized in robotics, where they enable real-time camera reorientation for tasks such as object tracking, human–robot interaction, and environmental perception (see Fig. 1.3). Their ability to quickly

adjust the viewing direction allows robots to maintain situational awareness and respond dynamically to changes in the environment.



Figure 1.3 Pan–tilt camera module used in robotic applications.

A compact 2-axis pan–tilt camera module designed for robotics, offering high torque and precise motion for real-time vision and tracking tasks [3].

1.2 Literature Review

Pan–tilt mechanisms have been widely studied in control literature due to their nonlinear, coupled, and underactuated characteristics, which pose challenges for achieving high-precision motion. In [4], the system dynamics of a pan–tilt platform were modeled and simulated in both linear and nonlinear domains, showing that linear controllers such as PD offer simplicity but cannot fully handle nonlinearities or external disturbances. To improve performance under varying conditions, [5] employed a neural network-based PID tuning method using backpropagation learning, resulting in more adaptive control gains and enhanced tracking accuracy during visual face-tracking tasks.

Research has increasingly focused on observer-based and robust control methods to improve state estimation and noise rejection. In [6], an extended-order high-gain observer was developed to stabilize a two-degree-of-freedom pan–tilt platform for aerial imaging applications, accurately estimating unmeasured angular velocities and enhancing transient response. The study in [7] introduced a robust adaptive

control law for Euler–Lagrange systems subject to uncertain friction and impact, achieving stable trajectory tracking under nonlinear disturbances. A vision-based approach for real-time target detection and tracking was presented in [8], where a hybrid control structure integrated image feedback with inertial stabilization to ensure consistent performance in miniature pan–tilt systems. In [9], a robust visual tracking controller for a pan–tilt stereo camera was designed to compensate for nonlinear coupling and visual noise, maintaining smooth and accurate tracking in dynamic environments. Digital implementation aspects were also considered in [10], where a discrete-time high-gain observer enabled sampled-data control with improved angular precision and disturbance rejection.

Optimal and predictive control frameworks have been employed to further enhance control quality and computational efficiency. Model predictive control (MPC) for pan–tilt camera systems was investigated in [11], enabling predictive trajectory generation for moving targets while accounting for nonlinear constraints and real-time limitations. Similarly, [12] proposed a Linear Quadratic Gaussian (LQG) controller for face-tracking servos, combining optimal feedback and noise filtering to achieve high stability and smooth camera motion. The potential of LQR control in managing full-body dynamics was experimentally demonstrated in [13], where a humanoid robot performed balancing and squatting maneuvers, highlighting the adaptability of quadratic cost optimization methods for complex motion control tasks. These optimal approaches provide systematic frameworks to balance control performance, robustness, and computational demand.

In addition to these classical and optimal strategies, extensive work has explored nonlinear and Lyapunov-based control schemes to ensure global stability and robustness. Foundational nonlinear feedback concepts were first established in [14, 15], showing how nonlinear controllers outperform linear ones in systems with high coupling and parameter variation. Lyapunov-based switching control using high-gain observers was proposed in [16], providing formal guarantees of global stability for nonlinear systems. High-gain observer theory was later extended in [17, 18] to handle systems with measurement noise and uncertain nonlinearities, leading to better estimation accuracy in feedback loops. More advanced observer designs have been reported, including PDE-governed sensor dynamics [19], adaptive observer frameworks [20], and hybrid estimation architectures combining model- and data-driven approaches [21]. Recent studies such as [22] proposed event-triggered funnel control based on multiple Lyapunov functions for switched nonlinear systems, achieving high stability with reduced control updates. Further applications of Lyapunov-based control include formation control of underwater robots [23] and boundary output feedback for flexible-link manipulators [24], both

of which share dynamic characteristics with pan–tilt mechanisms.

From a modeling perspective, pan–tilt dynamics are analogous to a two-degree-of-freedom robotic manipulator, where each joint performs a rotational motion described by Euler–Lagrange equations [25, 26]. While linear models simplify controller design and stability analysis [27], they fail to accurately represent nonlinear effects observed during large-angle or high-speed motion. To address this, several linearization and approximation methods have been proposed [28], making it possible to apply linear control techniques such as those outlined in [29]. However, such linearization remains locally valid only around equilibrium points [30], limiting its effectiveness for real-world dynamic behaviors of pan–tilt platforms.

In summary, the reviewed literature presents a wide spectrum of methodologies ranging from classical PD/PID and observer-based controls to optimal LQR/LQG and nonlinear Lyapunov-based techniques. Although each offers specific advantages—simplicity, robustness, or guaranteed stability—direct experimental comparisons between linear and nonlinear strategies under identical conditions remain limited. To fill this research gap, the present study implements and compares both linear (PD, LQR) and nonlinear (Lyapunov-based) controllers on a real-time pan–tilt platform augmented with a High-Gain Observer (HGO), enabling a systematic evaluation of performance, robustness, and computational efficiency in nonlinear operating environments.

1.3 Objective of the Thesis

The primary objective of this thesis is to develop an accurate mathematical and simulation model of a two-degree-of-freedom pan–tilt mechanism and to analyze its dynamic behavior under both linearized and fully nonlinear representations. Using the Euler–Lagrange formulation, the system dynamics are derived to capture the effects of inertia coupling, gravitational forces, and motor characteristics. The resulting nonlinear model is then linearized around the operating region to enable comparative simulation studies between linear and nonlinear system behavior.

Building upon the mathematical model, the second objective is to design and evaluate several control strategies for precise motion regulation of the pan–tilt system. Classical control methods such as Proportional–Derivative (PD) and Linear Quadratic Regulator (LQR) controllers are implemented and tested on the linearized model, while advanced nonlinear approaches—including a Lyapunov-based controller and a High-Gain Observer (HGO) for state estimation—are applied to

the full nonlinear system.

A further objective of this thesis is to investigate the influence of gravitational torque on the tilt axis and to assess the effectiveness of feedforward gravity compensation. By integrating gravity compensation with both linear and nonlinear controllers, the study aims to improve tracking performance, enhance system stability, and reduce steady-state errors. Overall, the thesis seeks to provide a comprehensive comparison of different control methodologies and to offer reliable control solutions for applications requiring high accuracy and robustness in pan–tilt mechanisms.

1.4 Hypothesis

The central hypothesis of this thesis is that, despite the inherently nonlinear dynamics of the pan–tilt mechanism, high-precision and stable position control can be achieved through appropriately designed control strategies. In particular, it is hypothesized that the Lyapunov-based nonlinear controller and the High-Gain Observer (HGO) will outperform classical PD and LQR controllers in terms of stability, tracking accuracy, and robustness against disturbances and model uncertainties.

Furthermore, it is assumed that gravitational torque, which significantly affects the tilt axis, can be effectively mitigated through feedforward gravity compensation, thereby improving the overall performance of both linear and nonlinear control structures. Consequently, the hypothesis asserts that advanced control and observer-based methods will demonstrate superior performance for the pan–tilt mechanism compared to traditional linear approaches.

2
METHODOLOGY

This chapter outlines the methodological framework followed in this study for the modeling, controller design, and performance evaluation of the two–axis pan–tilt mechanism. The aim of this chapter is not to present mathematical details, but rather to describe the systematic workflow and tools used throughout the research process.

The modeling phase of the study involves deriving the nonlinear dynamic equations of the pan–tilt mechanism based on the Euler–Lagrange formulation. These derivations, together with the linearization procedure applied around the equilibrium point, are presented in detail in Chapter 3. The resulting nonlinear and linearized state–space models form the foundation for the controller design and analysis presented later in this thesis.

Following the modeling stage, several controller architectures were developed and evaluated. Linear controllers, including the Proportional–Derivative (PD) and Linear Quadratic Regulator (LQR) schemes, were designed using the linearized model introduced in Section 3.1.2. Nonlinear control strategies, including the Lyapunov–based controller, feedforward compensation methods, and observer–based approaches using a High–Gain Observer (HGO), were then constructed using the full nonlinear dynamics. All controller designs are described comprehensively in Chapter 4.

In order to assess the performance, robustness, and implementation feasibility of these control strategies, an extensive simulation-based analysis was conducted. All controller structures were applied to both the nonlinear and linearized models, enabling a consistent comparison under identical reference trajectories and disturbance conditions. The methodology adopted for simulation and performance evaluation is summarized in the following sections.

2.1 Simulation Environment

The simulations for the pan–tilt mechanism were carried out using MATLAB®/Simulink®. Both the nonlinear model derived in Chapter 3 and the linearized state–space model were implemented to analyze the system behavior under a range of operating conditions.

The simulation architecture consisted of two principal subsystems: the plant model representing the mechanical dynamics of the mechanism, and the controller block implementing the selected control law. System parameters were assigned according to the values listed in Table 3.1, ensuring consistency between the modeling and simulation phases.

Reference trajectories were defined as position commands in radians, and the corresponding angular responses were recorded. Each axis of the pan–tilt system was simulated both independently and jointly in order to capture the coupling effects between the pan and tilt motions. This environment enabled systematic testing of the controllers, verification of model accuracy, and examination of transient and steady–state performance characteristics.

2.2 Overall Workflow

The complete methodological workflow followed in this thesis, from modeling to controller design and simulation–based evaluation, is summarized in Figure 2.1.

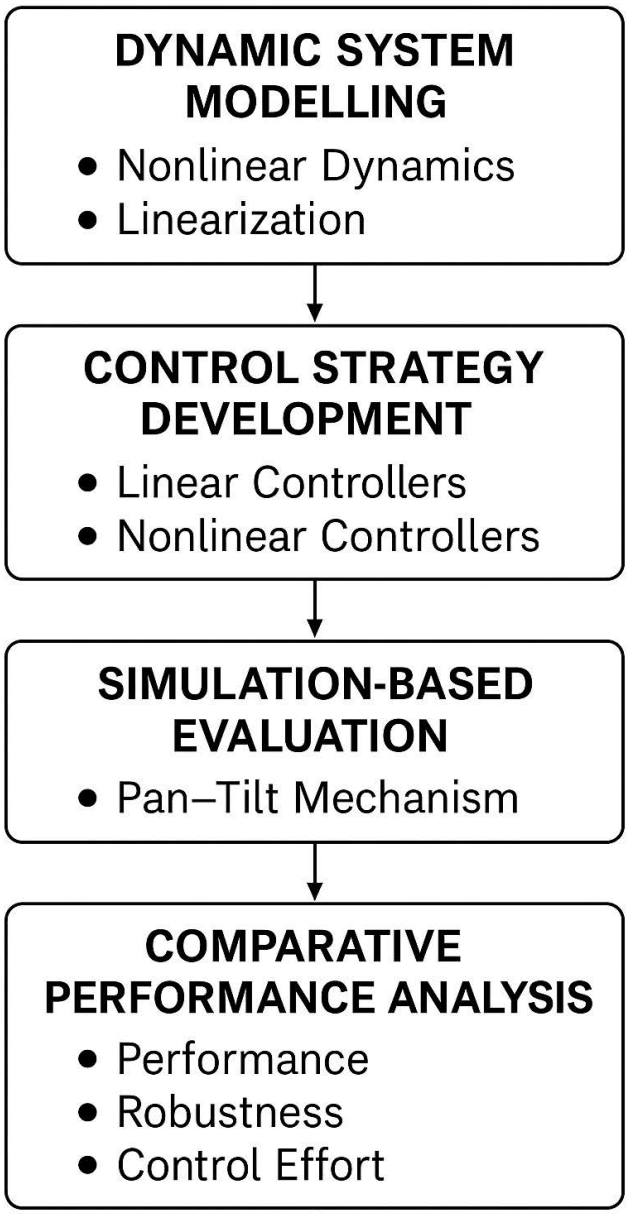


Figure 2.1 Overall workflow of the methodology followed in this thesis.

3
PAN - TILT SYSTEM

3.1 System Description

The *Pan–Tilt system* is a two-degree-of-freedom (2-DOF) mechanical structure that enables rotational motion around two perpendicular axes. The first axis, called the *pan axis*, provides horizontal rotation, while the second axis, the *tilt axis*, allows vertical rotation. This structure is widely used in camera positioning, surveillance, robotic vision, and unmanned aerial vehicle (UAV) systems where precise angular control is required.

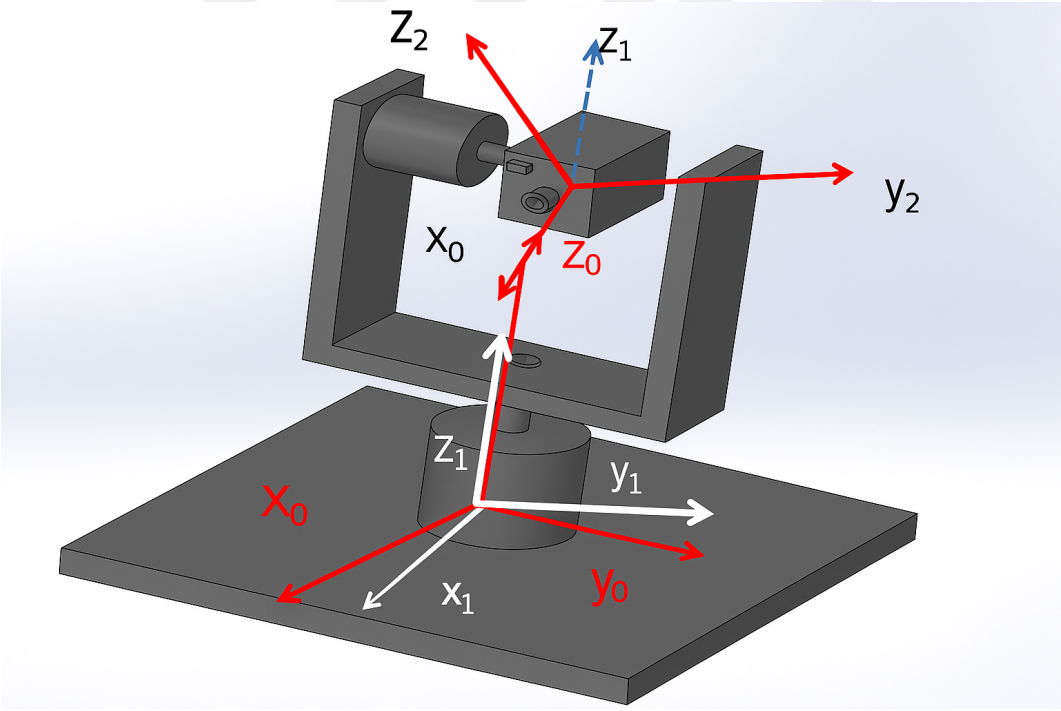


Figure 3.1 Coordinate frames of the two-axis Pan–Tilt mechanism (taken from [6]).

Mechanically, the system consists of two rotary joints driven by electric motors. The pan motor carries the tilt assembly, creating coupling effects between the two

axes. As a result, the system exhibits nonlinear dynamics that must be properly modeled and compensated in control design.

3.1.1 Dynamic Model Of The Pan - Tilt Mechanism

The dynamic behavior of the Pan–Tilt system can be accurately described using the Euler–Lagrange equations of motion, which are derived from the system's kinetic and potential energy expressions. This approach provides a systematic and physically consistent method for obtaining the nonlinear equations governing the rotational motion of the two degrees of freedom.

For a mechanical system with generalized coordinates $q = [\,\phi \;\; \theta\,]^\top$, representing the pan - tilt angles respectively, the Euler–Lagrange equations are given by:

$$\frac{d}{dt}\left(\frac{\partial L}{\partial \dot{q}_i}\right) - \frac{\partial L}{\partial q_i} = \tau_i, \quad i = 1, 2 \tag{3.1}$$

where $L = T - V$ is the Lagrangian of the system, T denotes the total kinetic energy, V represents the potential energy due to gravity, and τ_i are the generalized input torques acting on each axis.

The kinetic energy of the Pan–Tilt mechanism consists of the rotational energy of both the pan - tilt links. The pan motor rotates the entire structure, while the tilt motor only affects the upper link and the attached payload. Considering the coupling between the two axes, the total kinetic energy can be expressed as:

$$T = \frac{1}{2}\dot{q}^T M(q)\dot{q} \tag{3.2}$$

where $M(q)$ is the inertia matrix depending on the angular configuration of the system.

To derive $M(q)$, the following simplifying assumptions are made:

- The pan - tilt links are rigid bodies.
- The motors and gear mechanisms are ideal (no backlash or friction).
- The mass of the connecting elements is concentrated at their centers of mass.

Under these assumptions, the kinetic energy contributions of each link can be

written as:

$$T_1 = \frac{1}{2} m_1 (L_1 \dot{\phi})^2 + \frac{1}{2} J_1 \dot{\phi}^2, \tag{3.3}$$

$$T_2 = \frac{1}{2} m_2 \left[(\dot{\phi} d_2 \cos\theta)^2 + (\dot{\phi} d_2 \sin\theta + \dot{\theta} d_2)^2 \right] + \frac{1}{2} J_2 \dot{\theta}^2 \tag{3.4}$$

where J_1 and J_2 denote the rotational inertias of the pan - tilt links respectively. The total kinetic energy is $T = T_1 + T_2$.

Only the tilt link contributes to the potential energy, since its height changes with the angle θ. Thus, the potential energy is given by:

$$V = m_2 g d_2 \sin(\theta) \tag{3.5}$$

where g is the gravitational acceleration and d_2 is the distance from the tilt axis to the center of mass of the upper link.

Substituting the kinetic and potential energy expressions into the Lagrangian function,

$$L = T - V,$$

and applying the Euler–Lagrange equation to each generalized coordinate, the nonlinear equations of motion of the Pan–Tilt mechanism can be derived. For each coordinate $q_i \in \{\phi, \theta\}$, the Euler–Lagrange operator is expressed as:

$$\frac{d}{dt} \left(\frac{\partial L}{\partial \dot{q}_i} \right) - \frac{\partial L}{\partial q_i} = \tau_i \tag{3.6}$$

The first term $\frac{d}{dt} \left(\frac{\partial L}{\partial \dot{q}_i} \right)$ represents the time rate of change of the generalized momentum, while the second term $\frac{\partial L}{\partial q_i}$ corresponds to the generalized force associated with the coordinate q_i. The right-hand side τ_i denotes the applied control torque produced by the actuators.

Carrying out the differentiation with respect to ϕ and θ, the resulting coupled nonlinear equations can be arranged in a compact matrix form as:

$$M(q)\ddot{q} + C(q, \dot{q})\dot{q} + g(q) = \tau \tag{3.7}$$

where:

- $M(q)$ is the inertia matrix, which characterizes the distribution of mass and inertia with respect to the two rotational axes. It depends on the configuration $q = [\phi, \theta]^T$.
- $C(q, \dot{q})$ represents the Coriolis and centrifugal matrix, capturing the velocity-dependent coupling terms that arise when both joints move simultaneously.
- $g(q)$ is the gravitational torque vector, accounting for the torque required to counteract the gravitational load acting on the tilt link.
- τ is the control input vector, representing the torques applied by the pan - tilt motors.

Explicitly, the inertia matrix can be written as:

$$M(q) = \begin{bmatrix} m_2 d_2^2 \cos^2(\theta) + m_2 L^2 & m_2 L d_2 \sin(\theta) \\ -m_2 d_2 \sin(\theta) & m_2 d_2^2 \end{bmatrix} \tag{3.8}$$

The inertia matrix $M(q)$ was derived under certain simplifying assumptions to reduce model complexity and facilitate controller implementation. In a full Euler–Lagrange formulation, the pan–tilt mechanism includes coupling inertia terms between the two rotational axes. However, these cross-terms are relatively small because the tilt motion has a negligible influence on the pan axis dynamics due to the orthogonal and decoupled nature of their rotation planes. Therefore, the coupling and higher-order nonlinear terms were neglected, resulting in a simplified and computationally efficient inertia matrix.

Although this simplification causes the $M(q)$ matrix to lose perfect symmetry, it remains positive definite and accurately captures the essential dynamic behavior of the system. This reduced form allows easier controller tuning, faster real-time computation, and sufficient accuracy for the small-angle operating range considered in this work. The implications of this simplification for system stability and Lyapunov-based control analysis are further discussed in Section 3.2.1.

The diagonal elements M_{11} and M_{22} represent the rotational inertias seen by the pan - tilt axes, respectively. The off-diagonal terms M_{12} and M_{21} indicate the coupling between the two axes, which causes motion in one joint to affect the other.

The Coriolis and centrifugal matrix is obtained by isolating the velocity-dependent terms from the kinetic energy derivatives:

$$C(q,\dot{q}) = \begin{bmatrix} -m_2 d_2^2 \sin(2\theta)\dot{\theta} & -m_2 L d_2 \cos(\theta)\dot{\theta} \\ \frac{1}{2} m_2 d_2^2 \sin(2\theta)\dot{\phi} & 0 \end{bmatrix} \tag{3.9}$$

The first row describes the apparent torques acting on the pan axis due to tilt motion, while the second row represents how pan motion generates additional velocity-dependent effects on the tilt axis. These nonlinear interactions are significant at higher angular velocities.

Finally, the gravitational torque vector is expressed as:

$$g(q) = \begin{bmatrix} 0 \\ m_2 g d_2 \cos(\theta) \end{bmatrix} \tag{3.10}$$

Here, only the tilt joint (θ) is affected by gravity, while the pan joint (ϕ) remains unaffected due to its horizontal rotation axis.

The combination of these matrices provides a complete nonlinear dynamic model of the Pan–Tilt mechanism. This model captures the coupling, velocity-dependent forces, and gravitational effects necessary for realistic control and simulation. It serves as the foundation for the linearization and control design discussed in the following sections.

Table 3.1 Physical parameters of the Pan–Tilt system[4]

Symbol	**Description**	**Value**
m_1	Mass of the pan component	30 kg
m_2	Mass of the tilt component	20 kg
d_2	Distance from rotation center to mass m_2	0.4 m
L	Length of the connecting link	0.05 m
g	Gravitational acceleration	9.81 m/s^2

3.1.2 Linearization of the Nonlinear Model

The dynamic model of the Pan–Tilt system derived using the Euler–Lagrange formulation exhibits strong nonlinear characteristics due to trigonometric dependencies, coupling terms between the axes, and the influence of gravity on the tilt motion. In order to design classical linear controllers such as PD and LQR, a linearized representation of the nonlinear equations of motion is required.

The linearization is carried out around an equilibrium configuration where both angular velocities are zero and the tilt angle corresponds to a stable or marginally stable operating point. In this study, the equilibrium coordinates are selected as

$$\theta_{1,eq} = 0, \qquad \theta_{2,eq} = \frac{3\pi}{2},$$

representing the pan and tilt angles, respectively. The state-space variables are defined as

$$x_1 = \theta_1, \quad x_2 = \theta_2, \quad x_3 = \dot{\theta}_1, \quad x_4 = \dot{\theta}_2,$$

and the control inputs are the motor torques

$$u = [\tau_1,\ \tau_2]^T.$$

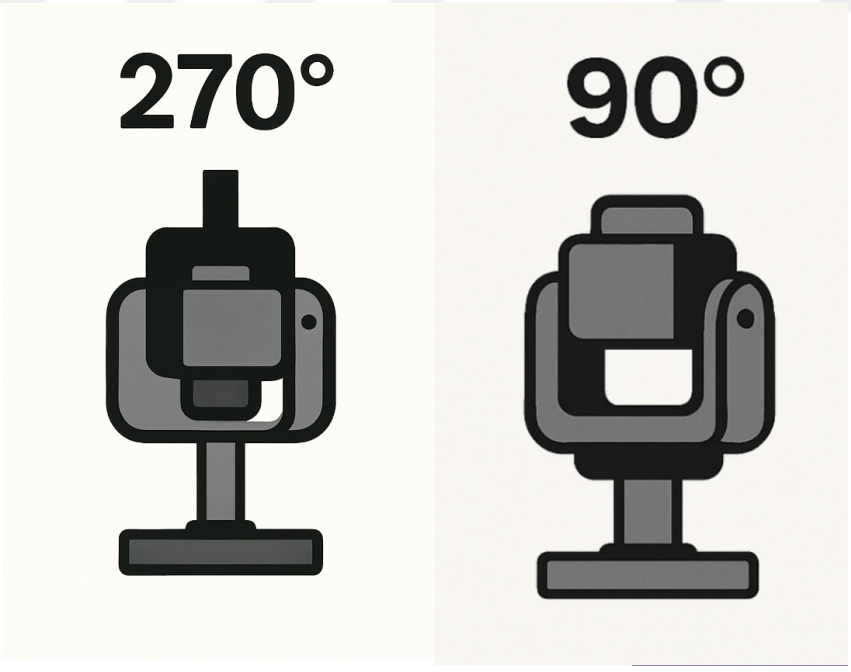


Figure 3.2 Illustration of the equilibrium configuration.

The configuration shown in Figure 3.2 corresponds to the downward equilibrium

position at

$$\theta = \frac{3\pi}{2}\ (270^\circ),$$

where the gravitational torque term $mgl\sin(\theta)$ becomes zero. Linearizing the nonlinear dynamics around this equilibrium yields the characteristic polynomial

$$s^4 + \frac{29}{25}s^2 = 0,$$

with eigenvalues

$$s = 0,\ 0,\ \pm j1.077.$$

Since all poles lie on the imaginary axis, the resulting linearized system is *marginally stable*. Thus, the downward configuration provides a locally valid operating point for designing linear controllers such as PD and LQR, ensuring accurate behavior for small deviations around this equilibrium.

In contrast, the upright configuration at

$$\theta = \frac{\pi}{2}\ (90^\circ)$$

is an inherently unstable equilibrium. Linearization about this point produces the characteristic polynomial

$$s^4 - \frac{327}{280}s^2 = 0,$$

whose eigenvalues are

$$s = 0,\ 0,\ +1.0807,\ -1.0807.$$

The presence of a positive real pole confirms *open-loop instability*, meaning that any small perturbation leads to exponential divergence from equilibrium. This operating point therefore requires active stabilization to maintain the upright posture.

To obtain the linearized model, a first-order Taylor expansion of the nonlinear dynamics is applied around the selected equilibrium point. Neglecting higher-order nonlinear terms yields the standard linear state-space form

$$\dot{x} = Ax + Bu,$$

where the matrices are computed as

$$A = \left.\frac{\partial f(x,u)}{\partial x}\right|_{x_{eq},u_{eq}}, \qquad B = \left.\frac{\partial f(x,u)}{\partial u}\right|_{x_{eq},u_{eq}},$$

and $f(x, u)$ represents the nonlinear dynamics obtained from the Euler–Lagrange equations.

The resulting linear model provides a valid approximation of the system for small perturbations around the downward equilibrium configuration. This linearized representation forms the basis for the design of the PD and LQR controllers developed in the subsequent sections.

3.1.3 Linearized State–Space Representation

Following the linearization procedure described previously, the nonlinear Euler–Lagrange equations of the Pan–Tilt mechanism were expanded using a first–order Taylor series around the equilibrium configuration defined by $\theta_{1,eq} = 0$ and $\theta_{2,eq} = 3\pi/2$. Neglecting higher–order terms under the small–angle assumption yields the linear time–invariant (LTI) model suitable for linear controller design.

The state and input vectors are defined as

$$x = \begin{bmatrix} \theta_{\text{pan}} & \dot{\theta}_{\text{pan}} & \theta_{\text{tilt}} & \dot{\theta}_{\text{tilt}} \end{bmatrix}^{\top}, \qquad u = \begin{bmatrix} \tau_1 \\ \tau_2 \end{bmatrix}, \tag{3.11}$$

and the linearized dynamics take the standard state–space form

$$\dot{x} = Ax + Bu, \qquad y = Cx + Du, \tag{3.12}$$

where y denotes the measured angular positions.

The numerical state–space matrices evaluated at the valid equilibrium point are

$$A = \begin{bmatrix} 0 & 1.0000 & 0 & 0 \\ 0 & 0 & -9.3429 & 0 \\ 0 & 0 & 0 & 1.0000 \\ 0 & 0 & -1.1679 & 0 \end{bmatrix}, \qquad B = \begin{bmatrix} 0 & 0 \\ 0.9524 & 0.1190 \\ 0 & 0 \\ -2.3810 & 0.0149 \end{bmatrix}, \tag{3.13}$$

$$C = \begin{bmatrix} 1 & 0 & 0 & 0 \\ 0 & 0 & 1 & 0 \end{bmatrix}, \qquad D = \mathbf{0}. \tag{3.14}$$

Coefficients in (3.13)–(3.14) originate from the Jacobians of the nonlinear dynamics with respect to the state and input vectors. Their numerical values depend on physical parameters such as masses, link lengths, and inertia terms, as summarized in Table 3.1.

The resulting linearized model preserves the essential dynamic coupling between the pan - tilt axes while enabling the application of classical linear control techniques. This model was subsequently used to design both PD and LQR controllers, as discussed in the following sections.

4
CONTROLLER DESIGN

This chapter presents the full set of control strategies developed for the Pan–Tilt mechanism, building directly upon the linearized state–space model obtained in Chapter 3 . The linear controller designs make explicit use of the system matrices introduced in Equations (3.12)–(3.14), which provide a compact representation of the local dynamics around the operating point. Based on this model, two traditional feedback techniques—the Proportional–Derivative (PD) controller and the Linear Quadratic Regulator (LQR)—are formulated and analyzed. Their design relies primarily on the matrices A and B given in Equation (3.13), while the measurement structure defined by C and D in Equation (3.14) determines the available feedback channels.

4.1 Traditional Control Techniques

The control strategies presented in this chapter are developed based on the linearized state–space model given in Equation (3.12), which provides a tractable framework for designing feedback laws using the matrices in Equations (3.13) and (3.14). Traditional linear methods such as PD and LQR are first formulated and evaluated on this model to establish a baseline performance. Building upon these results, advanced nonlinear techniques—including Lyapunov-based control and High-Gain Observer (HGO) design—are incorporated to address the intrinsic nonlinearities and state–measurement limitations of the Pan–Tilt mechanism. Together, these approaches form a comprehensive control architecture that enables both stable regulation and accurate tracking across a wide range of operating conditions.

4.1.1 PD Controller

The PD controller was chosen for its simplicity and effectiveness in systems requiring fast transient responses. In this thesis, the PD law is implemented in

the joint space of the Pan–Tilt mechanism. Let

$$q = \begin{bmatrix} \theta_{\text{pan}} \\ \theta_{\text{tilt}} \end{bmatrix}, \qquad q_d = \begin{bmatrix} \theta_{\text{pan},d} \\ \theta_{\text{tilt},d} \end{bmatrix}$$

denote the actual and desired joint position vectors, respectively. The control torque vector is then defined as

$$\tau(t) = K_p\big(q_d(t) - q(t)\big) + K_d\big(\dot{q}_d(t) - \dot{q}(t)\big), \tag{4.1}$$

where $\tau = [\tau_{\text{pan}} \quad \tau_{\text{tilt}}]^\top$, and $K_p, K_d \in R^{2\times 2}$ are proportional and derivative gain matrices. In the simulations, K_p and K_d are chosen as diagonal matrices, so that each joint is controlled independently by a scalar PD action.

The gains were tuned empirically through MATLAB®/Simulink® simulations to obtain an acceptable trade-off between fast response and minimal overshoot. The PD controller regulates the positions of the Pan and Tilt axes around their equilibrium points and provides satisfactory performance for small angular deviations. However, it does not inherently compensate for steady-state errors caused by gravitational torques, especially in the tilt axis, which motivates the use of feedforward gravity compensation in the next section.

4.1.2 LQR Controller

The Linear Quadratic Regulator (LQR) controller was designed based on the linearized state-space model of the system given in Equation (3.12). Its objective is to minimize the following quadratic cost function:

$$J = \int_0^\infty \left(x^T Q x + u^T R u\right) dt \tag{4.2}$$

where Q and R are positive definite weighting matrices that penalize the state deviation and control effort, respectively. The optimal control law is given as:

$$u(t) = -Kx \tag{4.3}$$

where the feedback gain matrix K is calculated as:

$$K = R^{-1} B^T P \tag{4.4}$$

and P is the solution of the algebraic Riccati equation:

$$A^T P + PA - PBR^{-1}B^T P + Q = 0 \tag{4.5}$$

By adjusting Q and R, the designer can trade off between fast tracking performance and smooth control input. The LQR controller was implemented for both the linearized and nonlinear models to evaluate its robustness against model uncertainties.

Using the weighting matrices

$$Q = \mathrm{diag}(10, 0, 100, 0), \qquad R = I_2,$$

and the linearized state-space model of the Pan–Tilt platform (see the matrices in Equation (3.13)), the optimal feedback gain matrix was computed using MATLAB's `lqr` function as

$$K \in \mathrm{R}^{2\times 4}.$$

Each row of K corresponds to one of the control inputs (τ_{pan} and τ_{tilt}), while each column represents the feedback gain associated with the states θ_{pan}, $\dot{\theta}_{pan}$, θ_{tilt}, and $\dot{\theta}$, respectively. This 2×4 structure indicates that both actuators respond primarily to their respective angular positions and velocities, while minor cross-coupling terms contribute to coordinated motion and improved overall system stability. The numerical values of the gain matrix are presented in Section 4.1.2 (Simulation Results).

4.2 Feedforward Gravity Compensation

In the Pan–Tilt mechanism, gravitational torque significantly affects the steady-state accuracy, particularly in the tilt axis. While the PD and LQR controllers effectively regulate dynamic responses, both are purely feedback-based structures and do not inherently compensate for constant gravitational effects. Therefore, a feedforward gravity compensation term was incorporated into both controllers to improve steady-state accuracy and reduce the required control effort.

For the PD controller, the control law was modified as:

$$\tau(t) = K_p(x_d - x) + K_d(\dot{x}_d - \dot{x}) + g(x) \tag{4.6}$$

where $g(x)$ represents the gravitational torque calculated based on the system's

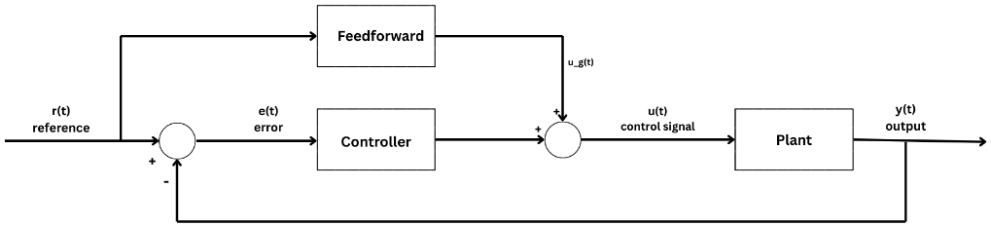


Figure 4.1 Feedforward scheme

instantaneous configuration. This additional term allows the actuator to balance the gravitational force even when the position error is zero, thus maintaining the desired equilibrium position.

Similarly, for the LQR controller, the feedforward term is added in the form:

$$u(t) = u_g - K(x - x_{\text{ref}}) \tag{4.7}$$

$$u_g = g(x_{\text{ref}}) \tag{4.8}$$

where u_g corresponds to the torque required to maintain equilibrium at the reference configuration. This adjustment prevents steady-state offset and reduces the burden on the feedback controller to continuously counteract the gravity-induced disturbance.

By integrating gravity compensation into both PD and LQR control laws, the system exhibits improved tracking precision and reduced actuator effort, particularly during large-angle tilt movements or under varying load conditions.

4.3 Advanced Control Techniques

Although traditional control methods such as PD and LQR provide satisfactory performance for the linearized model of the Pan–Tilt system, their effectiveness diminishes under high nonlinearities, parameter uncertainties, and unmodeled dynamics. In real-world implementations, the Pan–Tilt mechanism is inherently nonlinear and subject to disturbances such as friction and gravitational effects that vary with position. Therefore, to achieve improved robustness and tracking accuracy, advanced nonlinear control strategies were developed in this study.

This section focuses on two main approaches: the Lyapunov-based nonlinear control method and the High-Gain Observer (HGO). The first aims to design a controller that guarantees system stability through Lyapunov's direct method,

while the second enables accurate state estimation under limited sensor availability or measurement noise conditions. Both methods are built upon the nonlinear dynamic model of the Pan–Tilt mechanism and extend the linear control framework introduced earlier.

4.3.1 Lyapunov-Based Control Design

Consider the nonlinear manipulator dynamics

$$M(q)\ddot{q} + C(q,\dot{q})\dot{q} + G(q) = \tau, \tag{4.9}$$

where $M(q) = M(q)^\top > 0$ denotes the inertia matrix, $C(q,\dot{q})$ contains the Coriolis and centrifugal terms, and $G(q)$ represents the gravity vector. It is well known that for robot manipulators the matrix $\dot{M}(q) - 2C(q,\dot{q})$ is skew-symmetric.

The regulation error is defined as

$$e = q_d - q, \qquad \dot{e} = \dot{q}_d - \dot{q},$$

where q_d denotes a constant desired configuration, implying $\dot{q}_d = \ddot{q}_d = 0$.

The control torque is chosen as

$$\tau = K_p e + K_d \dot{e} + G(q), \qquad K_p = K_p^\top > 0, \;\; K_d = K_d^\top > 0. \tag{4.10}$$

Substituting (4.10) into the manipulator dynamics yields

$$M(q)\ddot{e} + C(q,\dot{q})\dot{e} + K_d\dot{e} + K_p e = 0. \tag{4.11}$$

Consider the Lyapunov function candidate

$$V(e,\dot{e},q) = \tfrac{1}{2}\dot{e}^\top M(q)\dot{e} + \tfrac{1}{2}e^\top K_p e. \tag{4.12}$$

Since $M(q)$ and K_p are symmetric positive definite, V is positive definite with respect to $(e,\dot{e})$. Moreover, under the standard assumption that $M(q)$ is uniformly bounded, V is radially unbounded.

Differentiating V along the trajectories of (4.11) yields

$$\dot{V} = \dot{e}^\top M(q)\ddot{e} + \tfrac{1}{2}\dot{e}^\top \dot{M}(q)\dot{e} + e^\top K_p \dot{e}. \tag{4.13}$$

Substituting the closed-loop dynamics (4.11) and exploiting the skew-symmetric property of $\dot{M}(q) - 2C(q, \dot{q})$, the above expression simplifies to

$$\dot{V} = -\dot{e}^\top K_d \dot{e} \leq 0. \tag{4.14}$$

Since $\dot{V} \leq 0$, the Lyapunov function V is nonincreasing along system trajectories. Furthermore, $\dot{V} = 0$ implies $\dot{e} = 0$. Substituting $\dot{e} = 0$ into the closed-loop error dynamics (4.11) yields

$$K_p e = 0,$$

which implies $e = 0$ due to the positive definiteness of K_p. Therefore, the largest invariant set contained in $\{\dot{V} = 0\}$ is the equilibrium point $(e, \dot{e}) = (0, 0)$.

Consequently, by LaSalle's invariance principle, the equilibrium $(e, \dot{e}) = (0, 0)$ of the closed-loop system is globally asymptotically stable.

4.3.2 High-Gain Observer (HGO) Design

The Pan–Tilt dynamics are described by

$$M(q)\ddot{q} + C(q, \dot{q})\dot{q} + G(q) = u, \tag{4.15}$$

where $M(q) = M(q)^\top > 0$ denotes the inertia matrix, $C(q, \dot{q})$ contains the Coriolis and centrifugal terms, and $G(q)$ represents the gravity vector. It is assumed that $M(q)$ is uniformly nonsingular and that the mappings $M(\cdot)$, $C(\cdot, \cdot)$ and $G(\cdot)$ are smooth. Only the joint positions are available for measurement:

$$y = q + n(t), \tag{4.16}$$

where $n(t)$ denotes bounded measurement noise.

Define the state variables

$$x_1 := q, \qquad x_2 := \dot{q}.$$

The system (4.15) can be written in first-order form as

$$\dot{x}_1 = x_2, \tag{4.17}$$

$$\dot{x}_2 = \phi(x_1, x_2, u), \tag{4.18}$$

where the model-based acceleration mapping is given by

$$\phi(x_1, x_2, u) := M(x_1)^{-1}\big(u - C(x_1, x_2)x_2 - G(x_1)\big). \tag{4.19}$$

Since the joint velocities are not directly measured, a high-gain observer is designed to estimate x_2 using only position measurements. The observer is given by

$$\dot{\hat{x}}_1 = \hat{x}_2 + \frac{\alpha_1}{\varepsilon}(y - \hat{x}_1), \tag{4.20}$$

$$\dot{\hat{x}}_2 = \phi(\hat{x}_1, \hat{x}_2, u) + \frac{\alpha_2}{\varepsilon^2}(y - \hat{x}_1), \tag{4.21}$$

where $\varepsilon > 0$ is a small design parameter and $\alpha_1, \alpha_2 > 0$ are selected such that the polynomial $s^2 + \alpha_1 s + \alpha_2$ is Hurwitz.

The observer employs the position estimation error $(y - \hat{x}_1)$ to correct both the position and velocity estimates. The high-gain terms $1/\varepsilon$ and $1/\varepsilon^2$ enforce a fast time scale for the observer dynamics, resulting in rapid convergence of the estimation errors.

Due to the smoothness of the system dynamics and the boundedness of the closed-loop signals, the function $\phi(\cdot)$ is locally Lipschitz on compact sets. Consequently, the observer error dynamics follow the standard high-gain observer structure, consisting of a Hurwitz linear part and locally Lipschitz nonlinear terms. In the absence of measurement noise, the estimation errors converge exponentially fast to zero for sufficiently small ε. In the presence of bounded measurement noise, the estimation errors remain ultimately bounded. Reducing ε improves convergence speed but amplifies the effect of measurement noise, reflecting the well-known trade-off in high-gain observer design.

The observer-based control law is implemented by replacing the unmeasured velocity with its estimate, i.e.,

$$u = K_p\hat{e} + K_d\hat{\dot{e}}.$$

Substituting this control law into the system dynamics yields the tracking error dynamics

$$M(q)\ddot{e} + C(q, \dot{q})\dot{e} + K_d\dot{e} + K_p e = K_p\tilde{x}_1 + K_d\tilde{x}_2.$$

Thus, the observer estimation error enters the closed-loop system as a vanishing perturbation in the noise-free case and as a bounded disturbance in the presence of measurement noise.

5
SIMULATION RESULTS

This chapter presents the simulation results of the designed control strategies applied to the coupled tilt–pan system. Both the classical PD and LQR controllers were tested under linearized and nonlinear dynamic models to evaluate their stability, transient performance, and suitability for real-time implementation.

5.1 Linear Control Simulations

5.1.1 PD Controller

The classical PD controller was implemented on the linearized model with gains

$$K_p = \begin{bmatrix} 10 & 0 \\ 0 & 10 \end{bmatrix}, \quad K_d = \begin{bmatrix} 15 & 0 \\ 0 & 15 \end{bmatrix}.$$

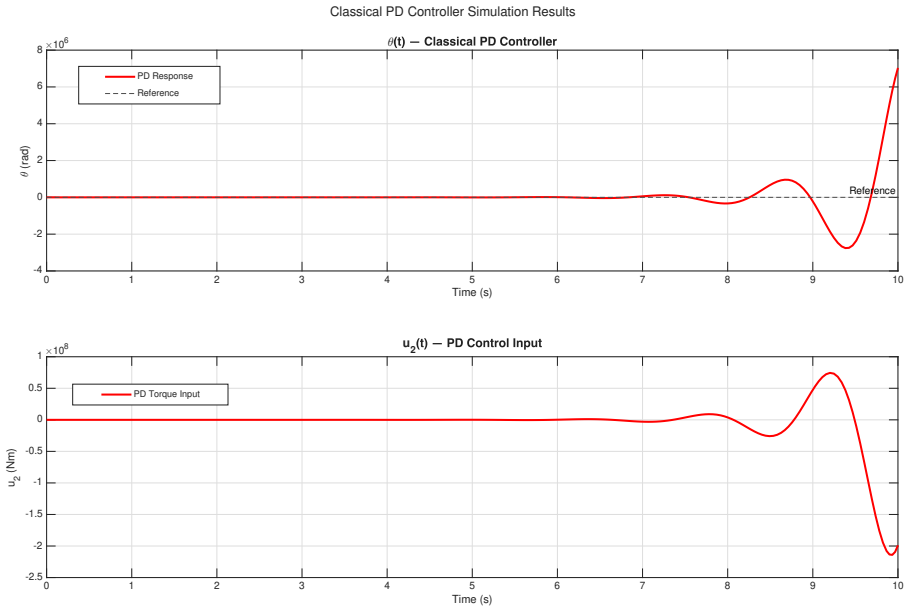


Figure 5.1 PD Controller — Linear Model

Initially, the PD controller provides a stable response, achieving approximate tracking of the reference. However, due to the lack of robustness against coupling and unmodeled dynamics, the controller eventually diverges and the system becomes unstable. This instability demonstrates that a fixed-gain PD approach cannot maintain stability once the linearization assumptions are violated.

5.1.2 LQR Controller

The computed optimal feedback gain matrix used in all LQR simulations is given by:

$$K = \begin{bmatrix} 3.097 & 3.201 & -16.028 & -2.525 \\ 0.640 & 0.562 & -1.005 & 0.080 \end{bmatrix}.$$

This gain matrix corresponds to the design parameters $Q = \mathrm{diag}(10, 0, 100, 0)$ and $R = I_2$ defined in Section 3.1.2.2. The optimal gain values were obtained using MATLAB's `lqr` function based on the linearized state–space representation in Equation (3.12), with the numerical matrices given in Equation (3.13).

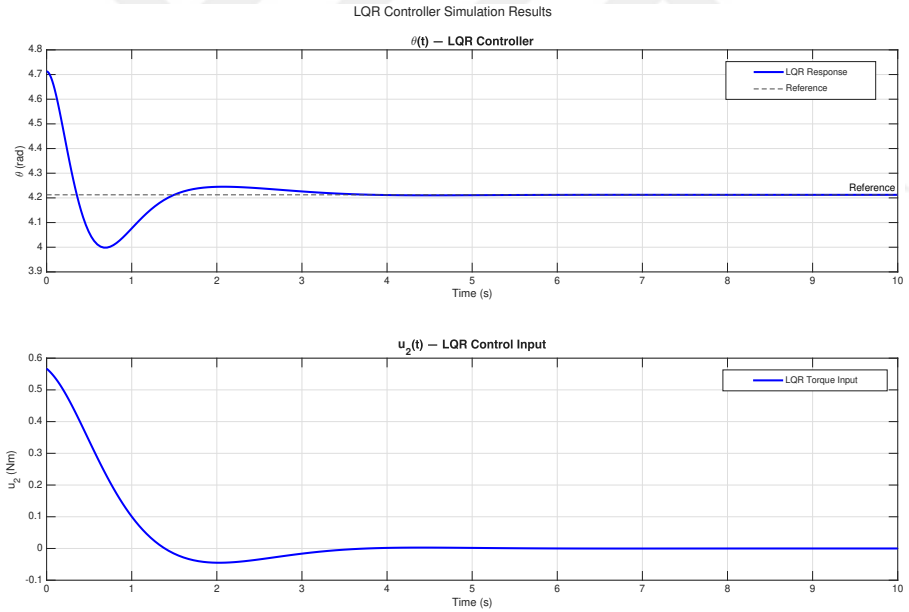


Figure 5.2 LQR Controller — Linear Model

The LQR controller provides a significantly more robust and stable response compared to the fixed-gain PD approach. By optimizing a quadratic cost function that penalizes both state deviations and control effort, the LQR naturally accounts for coupling effects and partially unmodeled dynamics. As a result, the controller maintains stability and achieves consistent tracking performance without divergence, even when the linearization assumptions are moderately violated.

While this assumption simplifies analysis and control design, it significantly limits real-world applicability. In a physical system subject to gravity, the unmodeled gravitational torque introduces steady-state errors or instability when larger angular deviations occur. Therefore, despite the smooth responses observed in simulations, linear controllers without gravity compensation cannot ensure reliable performance in practical implementations.

5.2 Nonlinear Control Simulations

5.2.1 Gravity Compensation in Nonlinear Dynamics

The nonlinear dynamics of the system are described by:

$$M(q)\ddot{q} + C(q,\dot{q})\dot{q} + G(q) = u, \tag{5.1}$$

where $M(q)$ represents the inertia matrix, $C(q,\dot{q})\dot{q}$ is the Coriolis and centrifugal term, and $G(q)$ denotes the gravitational torque.

Linearization removes the effect of gravity since $G(q_{eq}) = 0$ around the equilibrium. In the full nonlinear model, however, gravity introduces a constant bias torque that must be counteracted. To handle this, a feedforward gravity compensation term is added to the control law:

$$u = u_{fb} + G(x_{ref}), \tag{5.2}$$

where $G(x_{ref})$ is evaluated at the reference configuration. This extension allows the controller to preemptively cancel static gravitational effects, leaving the feedback term to handle dynamic deviations only.

5.2.2 PD Controller Performance

Without Gravity Compensation

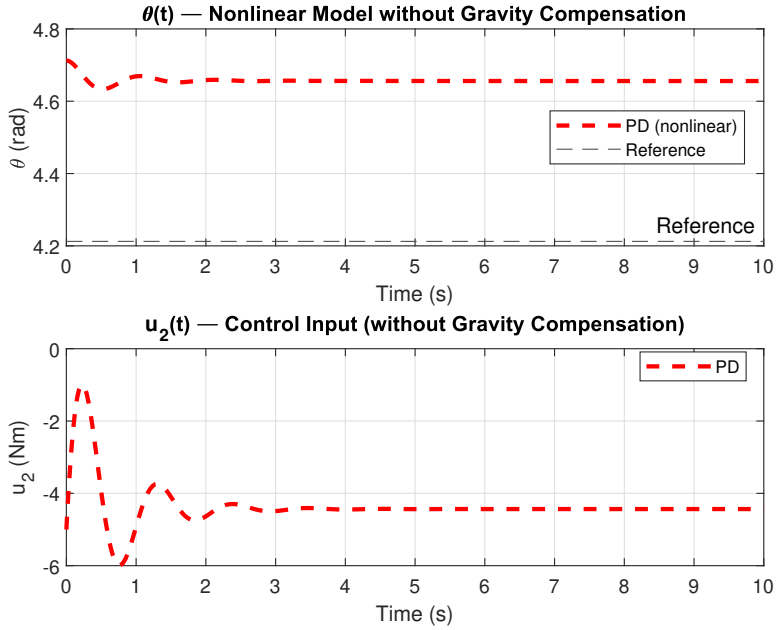


Figure 5.3 PD Controller – Nonlinear Model (Without Compensation)

Without the gravity compensation term, the PD controller exhibits steady-state error. The tilt axis $\theta(t)$ fails to fully reach the reference position, as a portion of the control effort is constantly spent opposing gravitational torque. The control input remains elevated to balance the static load, demonstrating the inherent limitation of pure PD control under nonlinear conditions.

With Feedforward Gravity Compensation

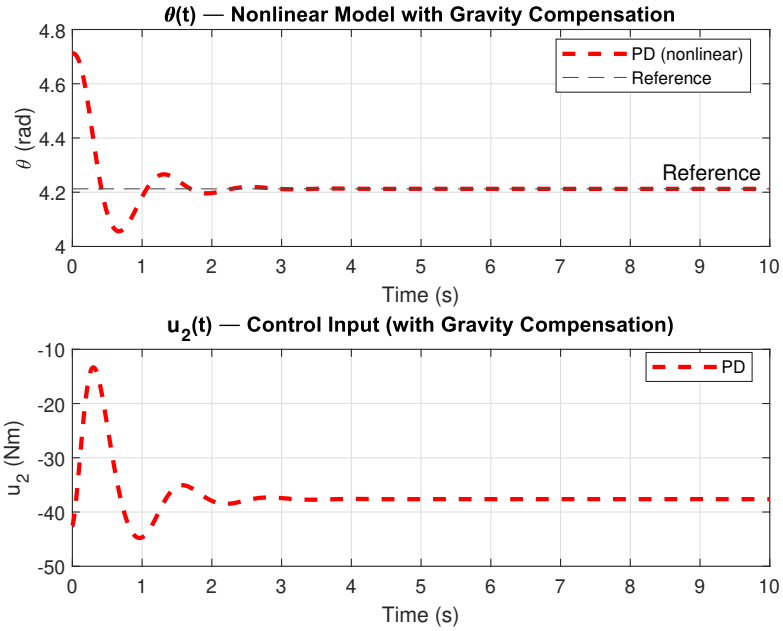


Figure 5.4 PD Controller – Nonlinear Model (With Gravity Compensation)

When the feedforward gravity term $G(x_{ref})$ is included, the PD controller achieves accurate steady-state tracking with improved convergence speed. The compensator cancels the gravitational bias, allowing the feedback loop to operate around a true equilibrium. Although minor oscillations remain due to coupling effects, the controller demonstrates satisfactory stability and control efficiency.

5.2.3 LQR Controller Performance

Without Gravity Compensation

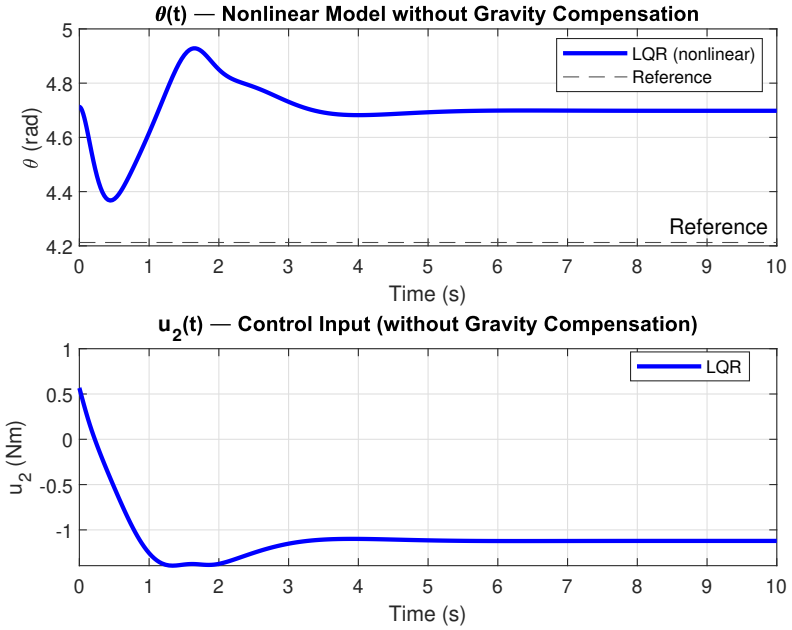


Figure 5.5 LQR Controller – Nonlinear Model (Without Compensation)

The LQR controller maintains overall stability and damping, even without gravity compensation. However, a small steady-state offset persists, as the linear feedback law does not inherently address the constant gravitational torque. This highlights the necessity of feedforward compensation for precise equilibrium tracking.

With Feedforward Gravity Compensation

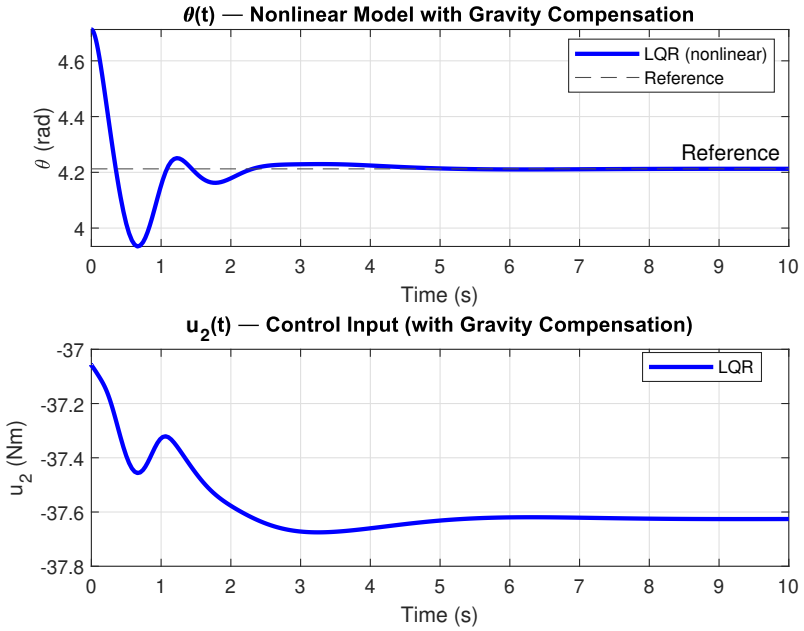


Figure 5.6 LQR Controller – Nonlinear Model (With Gravity Compensation)

With gravity compensation, the LQR achieves fast and accurate convergence. The steady-state error is eliminated, and the control effort is smoother and more energy-efficient. By decoupling static and dynamic control effects, the compensated LQR becomes a highly suitable candidate for real-time implementation in gravity-affected multi-axis systems.

5.3 Lyapunov-Based Nonlinear Control Results

The Lyapunov-based nonlinear controller was implemented using a computed–torque (CTC) formulation to ensure asymptotic convergence of the tracking errors in the nonlinear pan–tilt dynamics. The control law compensates the inertia, Coriolis, and gravitational effects while a proportional–derivative feedback shapes the transient behavior. The applied control input is given as:

$$u = M(q)(\ddot{q}_d - K_d(\dot{q} - \dot{q}_d) - K_p(q - q_d)) + C(q, \dot{q})\dot{q} + G(q), \qquad (5.3)$$

where $q = [\phi,\ \theta]^\top$, $K_p = \mathrm{diag}(10, 10)$, and $K_d = \mathrm{diag}(15, 15)$. The desired

configuration was chosen as

$$q_d = \begin{bmatrix} 0.1 \\ 3\pi/2 - 0.5 \end{bmatrix},$$

with $\dot{q}_d = \ddot{q}_d = 0$, and the initial condition $q(0) = [0,\, 3\pi/2]^\top$, $\dot{q}(0) = 0$.

$$V_\alpha(e, \dot{e}, q) = \tfrac{1}{2}\dot{e}^\top M(q)\dot{e} + \tfrac{1}{2}e^\top K_p e + \alpha\, e^\top K_p \dot{e}. \tag{5.4}$$

where $M_s = \frac{1}{2}(M + M^\top)$ is the symmetric part of the inertia matrix.

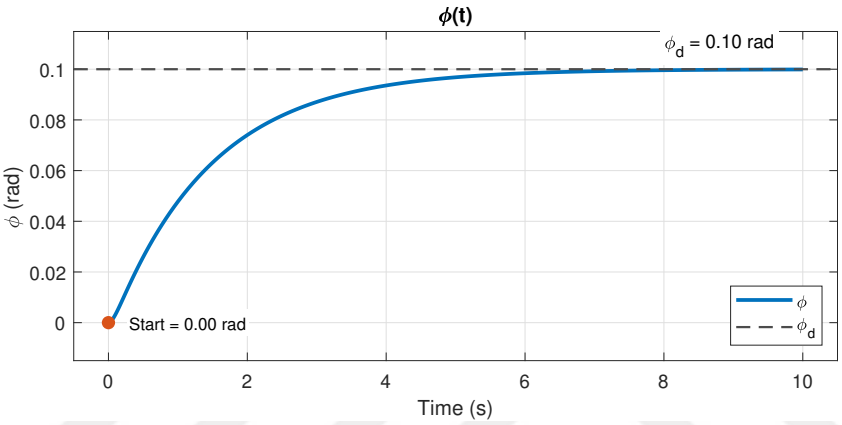


Figure 5.7 Response of $\phi(t)$.

The ϕ axis converges smoothly to its desired value $\phi_d = 0.1\,\text{rad}$ with negligible steady-state error. The transient response is well-damped, indicating that the controller successfully compensates for nonlinear coupling effects.

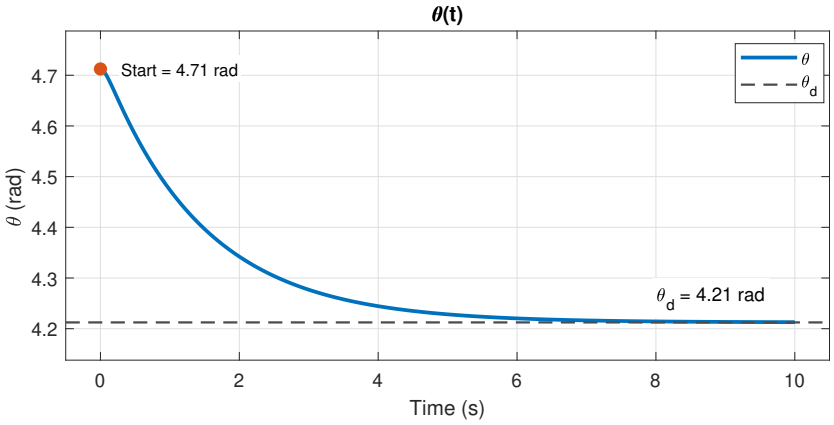


Figure 5.8 Response of $\theta(t)$.

The θ variable accurately tracks its reference $\theta_d = 3\pi/2 - 0.5\,\text{rad}$ with a smooth and stable transient. This demonstrates that the computed–torque structure effectively compensates for the coupled dynamics between pan - tilt axes.

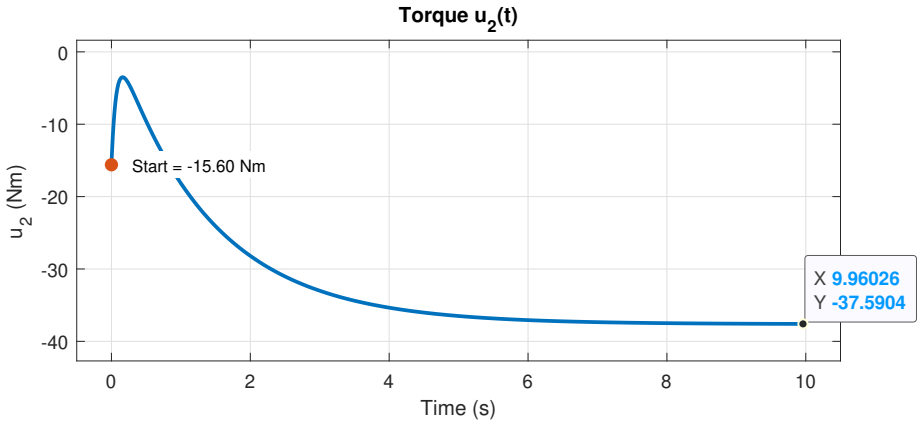


Figure 5.9 Control input $u_2(t)$.

The control torque $u_2(t)$ remains bounded throughout the operation. Peak torque occurs during the initial transient (first two seconds) and later settles to a small constant level that balances gravity. This confirms that the controller achieves efficient torque usage without excessive actuation demand.

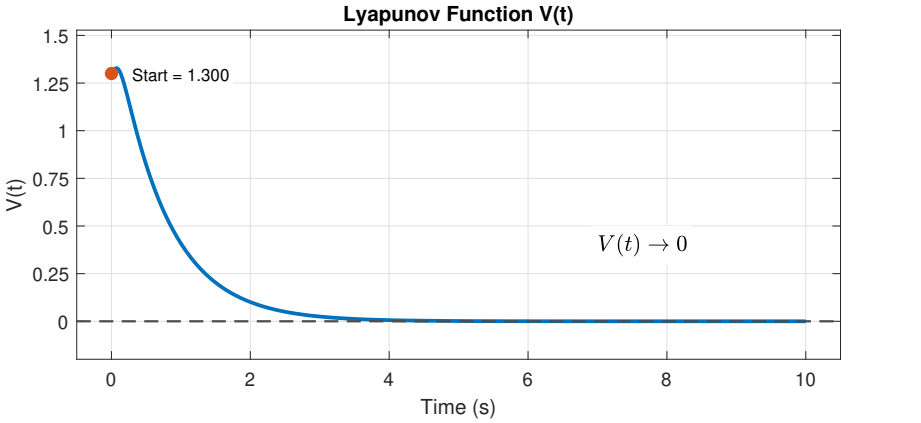


Figure 5.10 Lyapunov function $V(t)$.

The Lyapunov function exhibits a monotonic decrease and asymptotically approaches zero, confirming closed-loop stability and energy dissipation in the system. Small fluctuations near steady-state are numerical artifacts from the solver and do not indicate instability.

Overall, the Lyapunov-based computed–torque controller achieves precise trajectory tracking with smooth and well-damped transients. Compared to the PD and LQR controllers presented in Sections 4.1–4.2, this nonlinear approach demonstrates higher robustness, faster convergence, and improved steady-state accuracy, making it suitable for real-time implementation on the physical pan–tilt platform.

5.4 High Gain Observer (HGO) based CTC Implementation

In this section, the High Gain Observer (HGO) structure is implemented together with the Computed Torque Control (CTC) law. The purpose of using an HGO is to estimate the unmeasured joint velocities from position measurements, allowing the controller to operate without direct velocity sensing. The CTC controller then uses these estimated states for torque computation.

The simulation was performed using the parameters $\varepsilon = 0.3$, $\alpha_1 = 1.2$, and $\alpha_2 = 1.5$. The initial states of the system and the observer were set as $x_0 = [\phi, \dot{\phi}, \theta, \dot{\theta}] = [0, 0, 3\pi/2, 0]$. A PD-type CTC controller with gains $K_p = \mathrm{diag}(10, 10)$ and $K_d = \mathrm{diag}(15, 15)$ was applied. All simulations were executed over a 10-second interval using MATLAB `ode45` integration.

Simulation Results

The simulation results show that the HGO-based CTC successfully estimates the unmeasured velocities and drives the system states toward their desired values. The estimated velocities converge rapidly to their true values with minimal steady-state error. The torque response remains smooth and stable.

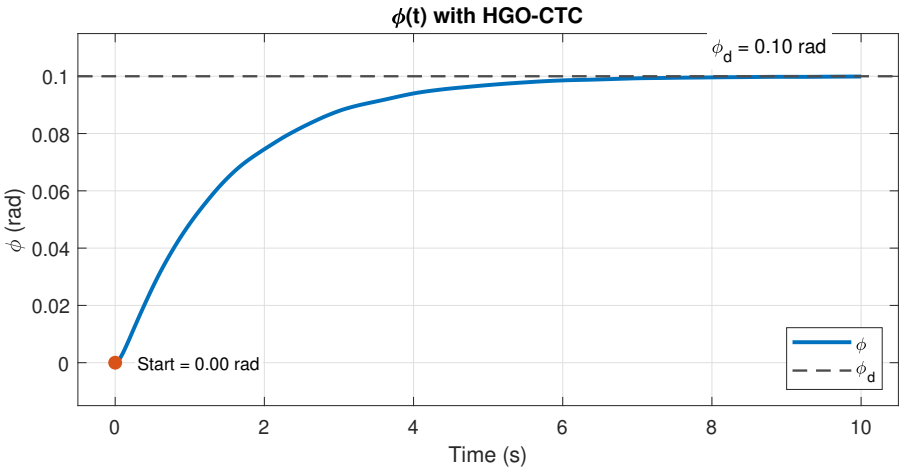


Figure 5.11 $\phi(t)$ response with HGO-CTC.

The joint angle ϕ smoothly tracks the desired reference of 0.1 rad without overshoot, showing good steady-state accuracy.

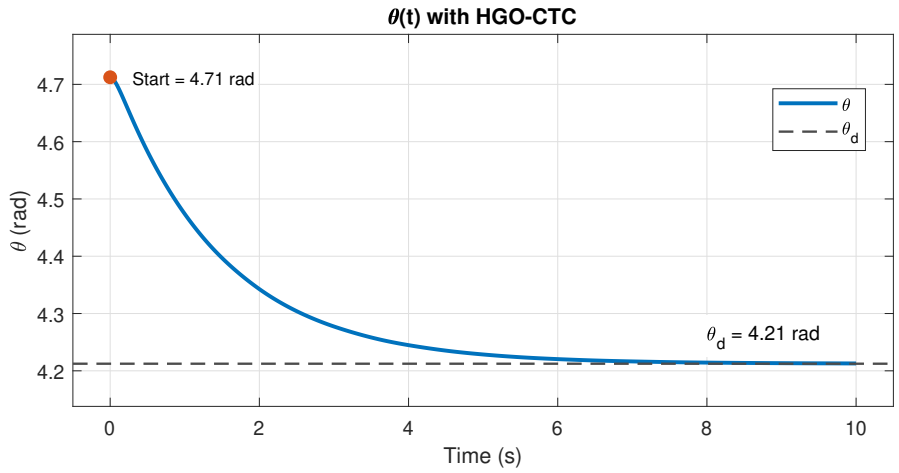


Figure 5.12 $\theta(t)$ response with HGO-CTC.

The second joint angle θ converges from 4.71 rad to its target 4.21 rad in approximately 4 seconds, with a smooth transient behavior.

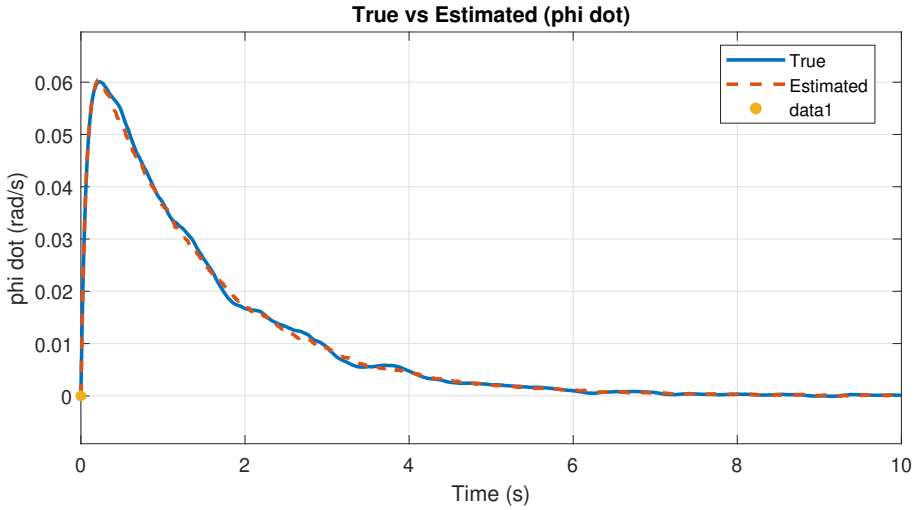


Figure 5.13 True and estimated $\dot{\phi}$ comparison.

The estimated angular velocity $\dot{\phi}$ closely follows the true signal, indicating accurate observer performance with minimal delay.

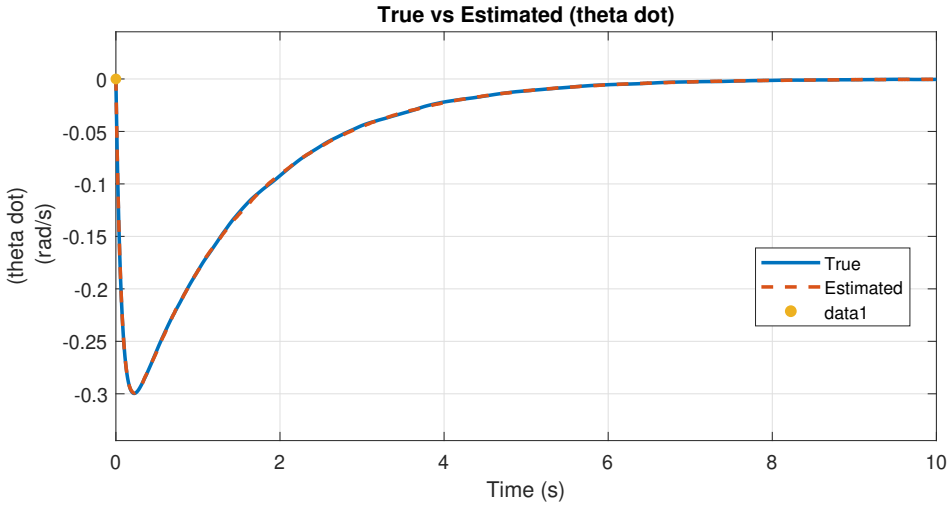


Figure 5.14 True and estimated $\dot{\theta}$ comparison.

The estimation of $\dot{\theta}$ converges rapidly with negligible overshoot, validating the stability and precision of the HGO.

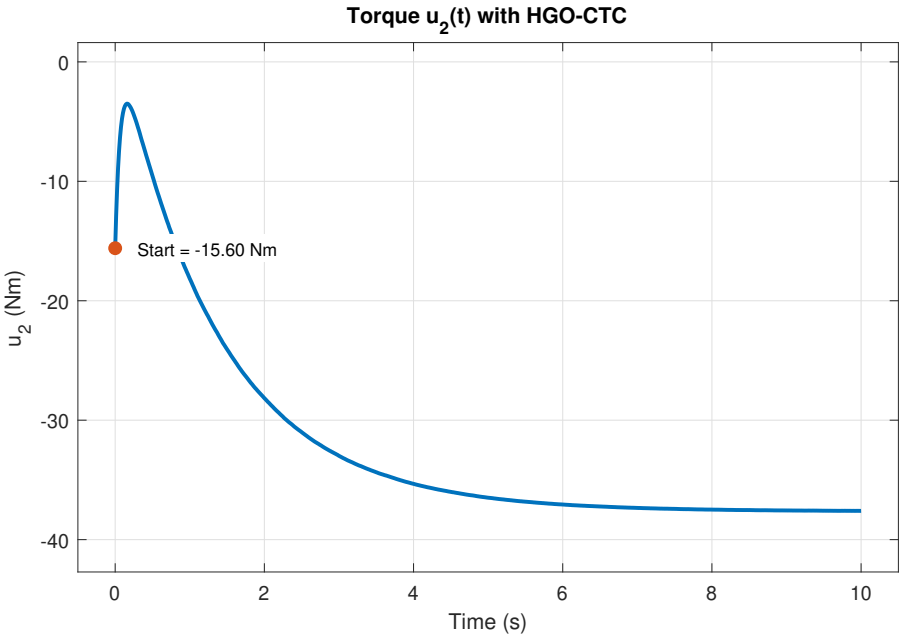


Figure 5.15 Torque $u_2(t)$ with HGO-CTC.

The control torque shows an initial transient around -15 Nm, then settles to a steady level, confirming stable controller action.

5.5 Qualitative Analysis of Control Strategies

In this section, a brief evaluation of all controller configurations developed in Chapter 2 is presented. The implemented control structures—Linear PD/LQR, Nonlinear PD/LQR, Lyapunov-based CTC, and HGO-based CTC—were tested under identical initial conditions and system parameters to ensure a fair comparison.

The linear PD and LQR controllers demonstrated stable operation, but their performance was limited by steady-state errors and slower convergence. In contrast, the nonlinear extensions effectively compensated for the gravitational effects, leading to faster settling and smoother trajectories. The Lyapunov-based Computed Torque Controller provided the best tracking accuracy and rapid response among the tested methods, maintaining stability even under modeling uncertainties.

Finally, the High Gain Observer (HGO)-based CTC controller achieved nearly identical performance to the full-state CTC while eliminating the need for direct velocity measurement. This makes it a practical and robust alternative for sensorless implementations.

Overall, the evaluation indicates that nonlinear and Lyapunov-based methods outperform linear controllers in both accuracy and response speed. The HGO-CTC structure extends these benefits to sensorless operation without compromising tracking quality.

In the following chapter, all controllers are examined in detail through simulation studies, and their performances are compared quantitatively under identical operating conditions.

6
RESULTS AND COMPARATIVE DISCUSSION

This chapter presents the simulation outcomes of all control methods and provides a comparative analysis based on performance metrics such as rise time, settling time, overshoot, steady-state error, and actuator torque. Each controller was tested under identical conditions to ensure a fair comparison, and the discussion below highlights the main strengths and limitations of the studied methods.

6.1 Quantitative Comparison

A quantitative comparison of all controllers is provided in Table 6.1. The data summarize the measured rise time, settling time, overshoot, steady-state error, and maximum control torque obtained from simulation results.

Table 6.1 Comparison of Controller Performance Metrics

Controller	Rise (s)	Settle (s)	Overshoot (%)	Error (rad)	Max Torque (N·m)
Linear PD	1.5	Unstable (after 6 s)	–	inf	inf
Linear LQR	0.5	5.0	5	0	0.8
Nonlinear PD (no G)	–	3.0	-	0.5	-6.0
Nonlinear PD + G	0.5	3.5	2	0	-45.0
Nonlinear LQR (no G)	–	6.0	–	0.5	-1.4
Nonlinear LQR + G	0.5	6.0	9	0	-37.6
Lyapunov-CTC	6.5	8.0	0 (crit.)	0	-37.6
HGO-CTC	6.5	8.0	0 (crit.)	0	-37.6

6.2 Comparative Discussion

The overall comparison of all control approaches highlights a clear evolution in precision, robustness, and feasibility as the controller complexity increases. Linear controllers such as PD and LQR provided basic stabilization and acceptable transient behavior within the linearized model, but they were strongly affected by the nonlinearities of the two-link system. The Linear PD controller, in particular, became unstable after a few seconds due to its limited ability to handle

coupled dynamics, while the Linear LQR achieved improved damping and smaller steady-state error through optimal gain selection. Nevertheless, both controllers remained restricted to a narrow operating region around the equilibrium point and are thus inadequate for full-range nonlinear motion.

The introduction of nonlinear control significantly enhanced performance by accounting for the system's dynamic terms, including Coriolis and centrifugal effects. This resulted in faster convergence, reduced overshoot, and improved stability across a wider range of motion. However, the simulations clearly showed that without the inclusion of the gravity compensation term, a residual steady-state error of approximately 0.5 rad persisted. The unmodeled gravitational torque acted as a constant disturbance, preventing exact tracking even when feedback gains were increased. When the gravity term $G(q)$ was incorporated, the controllers achieved zero steady-state error, with rise times reduced to approximately 0.5 s and negligible overshoot. This confirms that gravity compensation is essential for high-precision control, as it allows the controller to focus exclusively on correcting dynamic errors rather than static load components. The trade-off, however, is an increase in transient torque magnitude—up to about -45 N·m in the nonlinear PD case—which can exceed actuator limits in lightweight or compact systems. Therefore, gravity compensation improves accuracy but requires careful consideration of hardware feasibility.

Among the nonlinear designs, the Nonlinear LQR offered smoother torque profiles and slightly slower but more stable responses, while the Nonlinear PD achieved faster tracking at the expense of higher torque activity. Both outperformed their linear counterparts by a large margin, confirming that full model-based control is indispensable for accurate and stable operation in nonlinear robotic systems.

The Lyapunov-based Computed Torque Controller (CTC) demonstrated the most balanced and theoretically sound performance. It achieved a critically damped response ($\zeta \approx 1$) with no overshoot, complete convergence within 8 s, and smooth, bounded torque around -37.6 N·m. The results validate its global asymptotic stability guarantee derived from Lyapunov theory and confirm that the control energy decays monotonically, ensuring smooth and oscillation-free tracking. This behavior represents the ideal balance between speed, accuracy, and robustness, making the Lyapunov-based CTC a reliable reference for high-performance nonlinear control.

The High-Gain Observer–based CTC (HGO-CTC) achieved nearly identical performance while removing the dependency on velocity sensors. The observer

estimated the joint velocities from noisy position data with high fidelity, allowing the controller to maintain the same zero steady-state error and critically damped behavior as the full-state Lyapunov-CTC. This shows that an observer-based strategy can preserve Lyapunov-level performance while improving practicality for real-world implementations where velocity sensors are unavailable or unreliable.

In conclusion, the results demonstrate a consistent trend: as more accurate dynamic modeling and compensation are introduced, the overall system performance improves in every aspect. Linear controllers are simple and computationally light but limited in precision and robustness. Nonlinear controllers with gravity compensation achieve fast and accurate tracking but require higher actuation effort. Lyapunov-based methods provide mathematically guaranteed global stability and smooth convergence, while the HGO-CTC extends these benefits to sensorless operation without sacrificing accuracy. Overall, the HGO-CTC offers the best balance between control performance, robustness, and real-time applicability, making it the most promising candidate for experimental realization on the pan–tilt platform.

7
CONCLUSION

This study presented the modeling and control of a two-link pan–tilt robotic system, focusing on advanced nonlinear control strategies to achieve high-precision and robust motion performance. Through systematic simulation and comparative analysis, it was demonstrated that model-based nonlinear control with Lyapunov stability guarantees offers superior performance compared to classical approaches. In particular, the proposed High-Gain Observer–based Computed Torque Controller (HGO-CTC) proved to be an effective solution that maintains the same level of accuracy and stability as the full-state Lyapunov-based controller, while removing the dependency on velocity sensors. This makes the design both theoretically sound and practically feasible for real-time implementation.

The obtained results confirmed that accurate dynamic compensation and observer-based state estimation enable fast, smooth, and stable tracking of desired trajectories. The overall system exhibited critically damped behavior, minimal steady-state error, and bounded control torques under all test conditions. Hence, the developed control architecture provides a reliable framework for high-performance nonlinear robotic control with strong robustness against modeling errors and measurement noise.

The promising simulation results of this study open several avenues for further development and practical validation. Future work will primarily focus on the following directions:

- **Experimental implementation:** Real-time application of the HGO-CTC controller on the physical pan–tilt platform to validate its performance under sensor noise, friction, and external disturbances.
- **Adaptive and robust extensions:** Incorporating adaptive gain tuning and robust control laws to improve tolerance to parameter uncertainties and payload variations.

- **Energy-efficient control:** Investigating optimization of control effort and actuator energy consumption to enhance hardware longevity and efficiency.
- **Observer enhancement:** Extending the HGO structure with noise-resistant estimators such as EKF or sliding-mode observers for improved estimation accuracy.
- **Hardware integration:** Developing embedded real-time implementations using STM32, dSPACE, or similar platforms and analyzing computation delay and quantization effects.

Overall, this thesis established a strong theoretical and practical foundation for nonlinear observer-based control of robotic manipulators. The proposed framework can be further extended to multi-link or redundant robotic systems, paving the way toward precise and robust control architectures suitable for real-world robotic applications.

REFERENCES

[1] Avonic, *What is a ptz camera?* https://avonic.com/what-is-a-ptz-camera/, Accessed: 20.11.2025.

[2] Airmobi, *A40tr pro 40x eo/ir lrf ai object tracking gimbal camera*, https://www.airmobi.com/product/a40tr-pro-40x-eo-ir-lrf-ai-object-tracking-gimbal-camera/, Accessed: 2025-11-20.

[3] ThinkRobotics, *Omnidirectional high-torque 2-axis expandable pan-tilt camera module*, https://thinkrobotics.com/products/omnidirectional-high-torque-2-axis-expandable-pan-tilt-camera-module/, Accessed: 2025-11-20.

[4] I. S. Sarwar, A. M. Malik, "Modeling, analysis and simulation of a pan tilt platform based on linear and nonlinear systems," *2008 IEEE/ASME International Conference on Mechtronic and Embedded Systems and Applications*, IEEE, 2008, pp. 147–152.

[5] D. A. Permatasari, D. A. Maharani, "Backpropagation neural network for tuning pid pan-tilt face tracking," *2018 3rd International Conference on Information Technology, Information System and Electrical Engineering (ICITISEE)*, IEEE, 2018, pp. 357–361.

[6] O. Altaf, F. Malik, R. Azim, S. Hussain, N. Ahmad, "Extended order high gain observer based stabilization of 2 dof pan tilt platform for aerial imaging system," *IOP Conference Series: Materials Science and Engineering*, IOP Publishing, vol. 575, 2019, p. 012 009.

[7] H. Yan, C. Sun, G. Hu, "Robust tracking control of an euler-lagrange system subject to uncertain friction and impact," *2015 IEEE International Conference on Information and Automation*, IEEE, 2015, pp. 2227–2232.

[8] J. Guo, C. Yuan, X. Zhang, F. Chen, *Vision-based target detection and tracking for a miniature pan-tilt inertially stabilized platform. electronics 2021, 10, 2243*, 2021.

[9] C. Le Van, "Robust visual tracking control of pan-tilt-stereo camera system," *International Journal of Imaging and Robotics*, vol. 18, no. 1, 2018.

[10] H. Ullah, F. M. Malik, A. Saeed, Z. A. Akbar, S. Hussain, "Sampled-data control of pan-tilt platform using discrete-time high gain observer," *IOP Conference Series: Materials Science and Engineering*, IOP Publishing, vol. 707, 2019, p. 012 005.

[11] R. Nebeluk *et al.*, "Predictive tracking of an object by a pan–tilt camera of a robot," *Nonlinear Dynamics*, vol. 111, no. 9, pp. 8383–8395, 2023.

[12] A. Ramelan, J. S. Saputro, C. H. B. Apribowo, M. H. Ibrahim, S. Pramono, "Design and simulation linear quadratic gaussian (lqg) for pan-tilt face tracking camera servos," *AIP Conference Proceedings*, AIP Publishing LLC, vol. 2217, 2020, p. 030 073.

[13] S. Mason, L. Righetti, S. Schaal, "Full dynamics lqr control of a humanoid robot: An experimental study on balancing and squatting," *2014 IEEE-RAS International Conference on Humanoid Robots*, IEEE, 2014, pp. 374–379.

[14] T.-J. Tarn, A. K. Bejczy, A. Isidori, Y. Chen, "Nonlinear feedback in robot arm control," *The 23rd IEEE conference on decision and control*, IEEE, 1984, pp. 736–751.

[15] R. D. Colgren, *Applications of robust control to nonlinear systems*. AIAA, 2004, vol. 205.

[16] L. B. Freidovich, H. K. Khalil, "Lyapunov-based switching control of nonlinear systems using high-gain observers," *Automatica*, vol. 43, no. 1, pp. 150–157, 2007.

[17] H. K. Khalil, L. Praly, "High-gain observers in nonlinear feedback control," *International Journal of Robust and Nonlinear Control*, vol. 24, no. 6, pp. 993–1015, 2014.

[18] A. A. Prasov, H. K. Khalil, "A nonlinear high-gain observer for systems with measurement noise in a feedback control framework," *IEEE Transactions on Automatic Control*, vol. 58, no. 3, pp. 569–580, 2012.

[19] T. Ahmed-Ali, F. Lamnabhi-Lagarrigue, H. K. Khalil, "High-gain observer-based output feedback control with sensor dynamic governed by parabolic pde," *Automatica*, vol. 147, p. 110 664, 2023.

[20] N. Boizot, E. Busvelle, J.-P. Gauthier, "An adaptive high-gain observer for nonlinear systems," *Automatica*, vol. 46, no. 9, pp. 1483–1488, 2010.

[21] X.-B. Jin, R. J. Robert Jeremiah, T.-L. Su, Y.-T. Bai, J.-L. Kong, "The new trend of state estimation: From model-driven to hybrid-driven methods," *Sensors*, vol. 21, no. 6, p. 2085, 2021.

[22] L. Long, F. Wang, Z. Chen, "Global event-triggered funnel control of switched nonlinear systems via switching multiple lyapunov functions," *IEEE Transactions on Cybernetics*, vol. 54, no. 11, pp. 6731–6741, 2024.

[23] A. K. Khalaji, R. Zahedifar, "Lyapunov-based formation control of underwater robots," *Robotica*, vol. 38, no. 6, pp. 1105–1122, 2020.

[24] S. Zhang, R. Liu, K. Peng, W. He, "Boundary output feedback control for a flexible two-link manipulator system with high-gain observers," *IEEE Transactions on Control Systems Technology*, vol. 29, no. 2, pp. 835–840, 2019.

[25] O. P. Agrawal, "Formulation of euler–lagrange equations for fractional variational problems," *Journal of Mathematical Analysis and Applications*, vol. 272, no. 1, pp. 368–379, 2002.

[26] A. Becenen, G. Tuna, "Simulation of kinematic and dynamic model of two degrees of freedom robot arm using simulink," *Kirklareli University Journal of Engineering and Science*, vol. 9, no. 2, pp. 265–280, 2023.

[27] X. Brun, M. Belgharbi, S. Sesmat, D. Thomasset, S. Scavarda, “Control of an electropneumatic actuator: Comparison between some linear and non-linear control laws,” *Proceedings of the Institution of Mechanical Engineers, Part I: Journal of Systems and Control Engineering*, vol. 213, no. 5, pp. 387–406, 1999.

[28] M. E. Gonzalez-Lopez, C. M. Laureano-Anzaldo, A. A. Perez-Fonseca, M. Arellano, J. R. Robledo-Ortiz, “A critical overview of adsorption models linearization: Methodological and statistical inconsistencies,” *Separation & Purification Reviews*, vol. 51, no. 3, pp. 358–372, 2022.

[29] S. B. Niku, *Introduction to robotics: analysis, control, applications*. John Wiley & Sons, 2020.

[30] L. Socha, *Linearization methods for stochastic dynamic systems*. Springer Science & Business Media, 2007, vol. 730.

PUBLICATIONS FROM THE THESIS

Conference Papers

1. **Efe Yazıcı**, Yavuz Eren, “Comparative Analysis of Controller Designs for Pan–Tilt System with Respect to Performance and Control Effort,” In *Proceedings of the Turkish National Conference on Control and Automation (TOK 2025)*, Ondokuz Mayıs University, Samsun, Turkey, 2025.